4. X. Li, Z. Shao, Z. He, and C. You, Wideband bandpass filter integrating half mode substrate integrated waveguide with novel DGS cell, IEEE Int Conf Commun Probl Solving (2014), 661–664.
5. Z. Li, W. Shi, and Y. Yuan, A novel compacted microstrip bandpass filter using stepped impedance resonators (SIR) and defected ground structures (DGS), IEEE 15th Int Conf Electron Packing Technol (2014), 1338–1340.
6. S.S. Chen, L. Li, and Z.Y. Chen, A novel coupled-defected ground structure with enhanced coupling-coefficient and its application in filter design, Prog Electromagn Res Lett 52 (2015), 93–97.
7. J.S. Hong and B.M. Karyamapudi, A general circuit model for defected ground structures in planar transmission lines, IEEE Microw Wireless Comp Lett 15 (2005), 706–708.
8. J.S. Lim, C.S. Kim, Y.T. Lee, D. Ahn, and S. Nam, A spiral-shaped defected ground structure for coplanar waveguide, IEEE Microw Wireless Comp Lett 12 (2002), 330–332.
9. M.K. Mandal and S. Sanyal, A novel defected ground structure for planar circuits, IEEE Microw Wireless Comp Lett 16 (2006), 93–95.
10. J.S. Park, J.S. Yun, and D. Ahn, A design of the novel coupled-line bandpass filter using defected ground structure with wide stopband performance, IEEE Trans Microw Theory Tech 50 (2002), 2037–2043.
11. C. Kumar and D. Guha, Nature of cross-polarized radiation from probe-fed circular microstrip antennas and their suppression using different geometries of defected ground structures (DGS), IEEE Trans Antennas Propag 60 (2012), 92–101.
12. D.J. Woo, T.K. Lee, J.W. Lee, C.S. Pyo, and W.K. Choi, Novel U-slot and V-slot DGS for bandstop filter with improved Q factor, IEEE Trans Microw Theory Tech 54 (2006), 2840–2847.
13. E.K.I. Hamad, A.M.E. Safwat, and A.S. Omar, L-shaped defected ground structure for coplanar waveguide, IEEE Antennas Propag Soc Int Symp 2B (2005), 663–666.
14. L.H. Weng, Y.C. Guo, X.W. Shi, and X.Q. Chen, An overview on defected ground structure, Prog Electromagn Res B 7 (2008), 173–189.
15. Y. Guo and Q. Wang, An improved parameters extraction method for dumbbell-shaped defected ground structure, Engineering 2 (2010), 197–200.

SUBSTRATE INTEGRATED WAVEGUIDE CIRCULARLY POLARIZED HORN-DIPOLE ANTENNA WITH IMPROVED GAIN

Yu Luo and Jens Bornemann
Department of Electrical and Computer Engineering University of Victoria, Victoria, BC V8W 3P6, Canada; Corresponding author: j.bornemann@ieee.org

Received 17 May 2016

ABSTRACT: *A substrate integrated waveguide (SIW) horn antenna is combined with a dipole to achieve circular polarization (CP). First, it is established that CP can be achieved by combining a horn and a dipole. To excite the dipole, double-sided tapered and balanced transmission lines are employed at the central part of the horn aperture. Secondly, after the position and the size of the dipole are determined, a directional circularly polarized beam in the plane of the substrate is achieved. Finally, the proposed antenna is fabricated and measured. Experimental results are in good agreement with simulations. Measured results show that an effective bandwidth of 5% for axial ratio (AR) less than 3 dB and return loss (RL) better than 10 dB from 11.8 to 12.4 GHz is achieved. In particular, the maximum gain of the proposed antenna is as high as 7.5 dBi due to the design of the horn structure.* © 2016 Wiley Periodicals, Inc. Microwave Opt Technol Lett 58:2973–2977, 2016; View this article online at wileyonlinelibrary.com. DOI 10.1002/mop.30191

Key words: *substrate integrated waveguide; circularly polarization; horn antennas; satellite communications*

1. INTRODUCTION

The International Telecommunication Union (ITU) has allocated the 12-GHz-band for broadcasting satellite service (BSS) [1]. In order to reduce multipath effects and offer flexibility in orientation angle between receiving and transmitting antennas, circular polarization (CP) is widely used in satellite communication systems [2].

Substrate integrated waveguide (SIW) circuitry is a very promising candidate for communication technology, especially for systems operating in the millimeter-wave region. The most significant advantage of SIW is the possibility of integrating all components on a single substrate, including passive elements, active devices as well as antennas [3]. The SIW horn antenna, employed as one kind of typically planar horn antennas, exhibits attractive advantages of low profile, simple fabrication, and easy integration with other components, etc. [4–7]. Unfortunately, SIW horn antennas are inherently linearly polarized. On the other hand, several circularly polarized SIW antennas were presented with main beams perpendicular to the substrate [8–11].

To achieve CP in the horizontal plane, a rectangular waveguide combined with a printed dipole was proposed in Ref. [12]. However, this antenna does not permit low-cost fabrications due to its three-dimension (3D) structure. Printed magnetic dipoles combined with a loop [13] or a linear dipole [14] were designed and shown to exhibit directional beams parallel with substrates. However, the maximum gains of the two antennas are 2.6 dBi and 2.3 dBi. The relative effective bandwidth (the common overlapped bandwidth limited by the 3-dB AR and 10-dB RL) are 2.4% and 1.9%. In addition, the feed pins of the two antennas are vertical to the substrate, which leads to difficulties in integrating all components on the same substrate.

Therefore, in this paper, a SIW circularly polarized horn antenna in combination with a dipole is presented. In principle, this design is similar to that in Ref. [14]. However, two major changes are implemented. First, the SIW horn antenna is similar to a potter horn design in order to achieve a certain aperture distribution that results in higher gain. Secondly, to excite the dipole in the plane of the substrate, thus allowing for full printed-circuit board integration, double-sided tapered and balanced transmission lines are employed. Moreover, the position and size of the dipole, which is also designed using balanced transmission lines at the central part of the horn aperture, are investigated to obtain a directional circularly polarized beam parallel to the substrate. To verify the proposed design, the antenna is fabricated and measured. Measurements show good agreement with simulations, and high gain, low axial ratio as well as low reflection coefficients are achieved.

2. ANTENNA DESIGN

A SIW antenna and its distributions of the E-field magnitude in the aperture at 12 GHz are shown in Figure 1. Due to the Potter-horn design, the aperture field distribution resembles that of a TE_{30} mode with two zeros of the E-field. These are the two points at which the double-sided tapered and balanced transmission lines for the printed dipole are connected (Fig. 2). Thus the aperture distribution of the horn is maintained and remains uninfluenced by the dipole. The dipole is horizontally polarized, and the aperture is treated as two magnetic dipoles which are vertical polarized.

The two magnetic dipoles lead to high gains. E_θ and E_φ are the θ and φ components of the far-zone electric field, respectively (Fig. 2). In the yz-plane, E_θ is determined by the dipole and E_φ is determined by the aperture. Obviously, in broadside

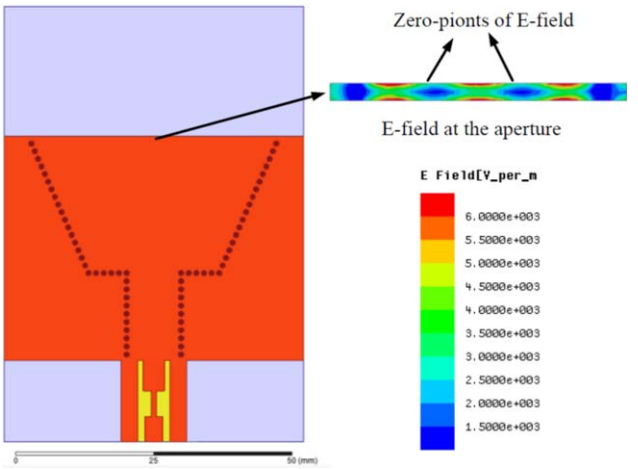

Figure 1 A SIW potter horn antenna and its distribution of complex magnitude E-field in the aperture at 12 GHz. [Color figure can be viewed at wileyonlinelibrary.com]

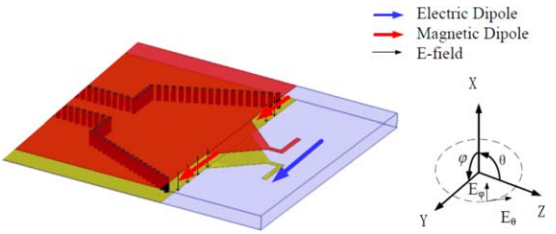

Figure 2 A conceptual design of a horn antenna combined with a dipole and its coordinate system. [Color figure can be viewed at wileyonlinelibrary.com]

direction, i.e., the z-axis, if E_θ and E_φ have the same magnitude and 90° phase difference, CP can be achieved. To obtain the same magnitude of E_θ and E_φ, the width of the end of the tapered lines at the aperture equals the distance between the two E-field zero points in Figure 1.

Based on the above discussion, a SIW CP horn antenna combined with a dipole is proposed and constructed as shown in Figure 3. The

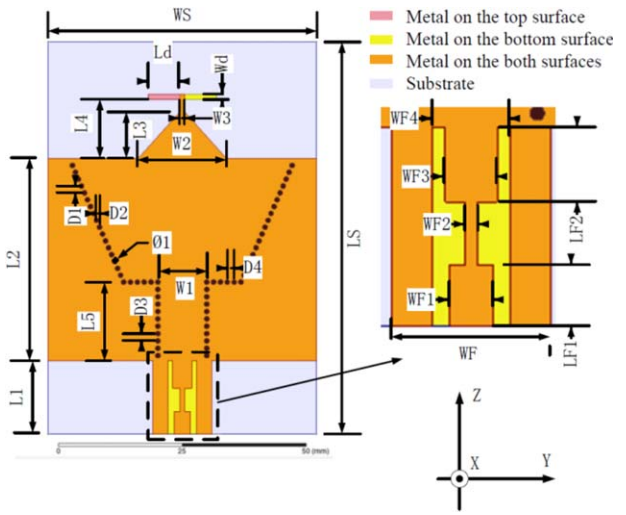

Figure 3 Geometry of the proposed antenna. [Color figure can be viewed at wileyonlinelibrary.com]

TABLE 1 Dimensional Parameter of the Proposed Antenna in Figure 3

Parameters	L_1	L_2	L_3	L_4	L_5	W_1	W_2	W_3
Value/mm	15	41.25	9.44	12	16	10	18	1
Parameters	L_d	W_d	D_1	D_2	D_3	D_4	Ws	Ls
Value/mm	6.5	1	1.4	0.616	1.5	1.4	55	80
Parameters	W_F	W_{F1}	W_{F2}	W_{F3}	W_{F4}	L_{F1}	F_{L2}	$Ø_1$
Value/mm	12	3.2	1	3.9	6	4.6	5.7	1

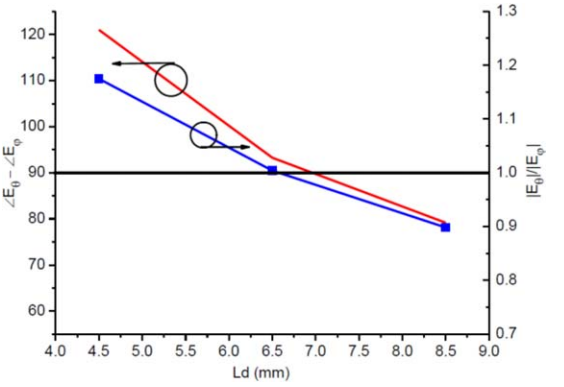

Figure 4 Phase difference ($\angle E_\theta - \angle E_\varphi$) and magnitude ratio ($|E_\theta|/|E_\varphi|$) in broadside direction, i.e., z-axis, as a function of L_d at 12 GHz. [Color figure can be viewed at wileyonlinelibrary.com]

antenna is designed on a Rogers 5880 substrate with relative permittivity of $\varepsilon_r = 2.18$ and thickness of 3.175 mm. A stepped-impedance grounded coplanar waveguide (GCPW) transmission line, e.g. [15], is employed to connect the SMA connector with the SIW and to obtain a good impedance match.

To achieve CP in the broadside direction, two parameters are varied: the length of the dipole ($2L_d$) and the distance between the dipole and the aperture, set as L_4 (Fig. 3).

Initially, the length of the dipole is selected as $\lambda_0/2$ where λ_0 is the wavelength in free space at the center frequency, i.e., 12 GHz. To achieve a 90° phase difference between E_θ and E_φ, the distance between the dipole and the aperture is investigated. On the z-axis, the field of the aperture lags that of the dipole. The phase difference of E_θ and E_φ due to the space position, $\Delta\phi_1$, is

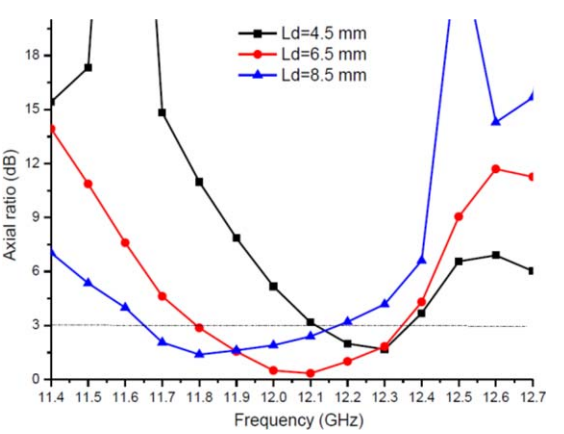

Figure 5 Axial ratios in broadside direction, i.e., z-axis, as a function of frequency versus different values of L_d. [Color figure can be viewed at wileyonlinelibrary.com]

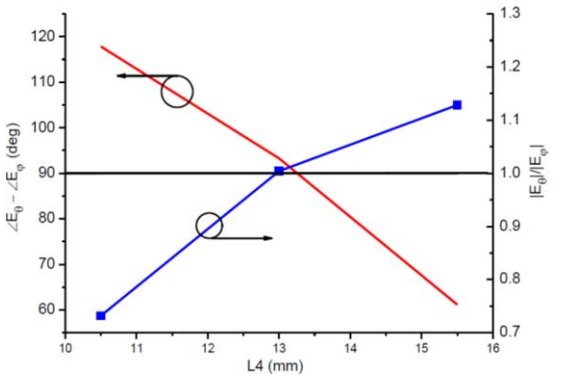

Figure 6 Phase difference ($\angle E_\theta - \angle E_\varphi$) and magnitude ratio ($|E_\theta|/|E_\varphi|$) in broadside direction, i.e., z-axis, as a function of L_4 at 12 GHz. [Color figure can be viewed at wileyonlinelibrary.com]

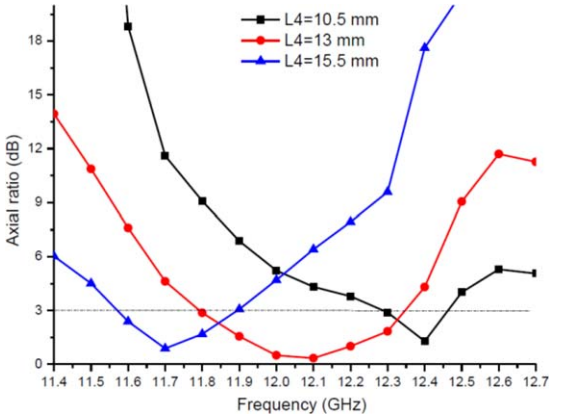

Figure 7 Axial ratios in broadside direction, i.e., z-axis, as a function of frequency versus different values of L_4. [Color figure can be viewed at wileyonlinelibrary.com]

$$\Delta\phi_1 = -2\pi\ L_4/\lambda_0 \tag{1}$$

On the other hand, it can be argued that the feed lines of the dipole make the E-field produced by the dipole lag that of the aperture. The phase difference of E_θ and E_φ due to the feed lines, $\Delta\phi_2$, is

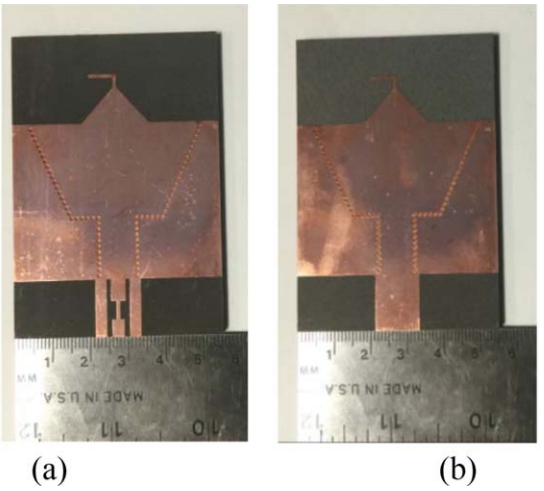

Figure 8 Top- and bottom-view photographs of the fabricated antenna; (a) top view, (b) bottom view. [Color figure can be viewed at wileyonlinelibrary.com]

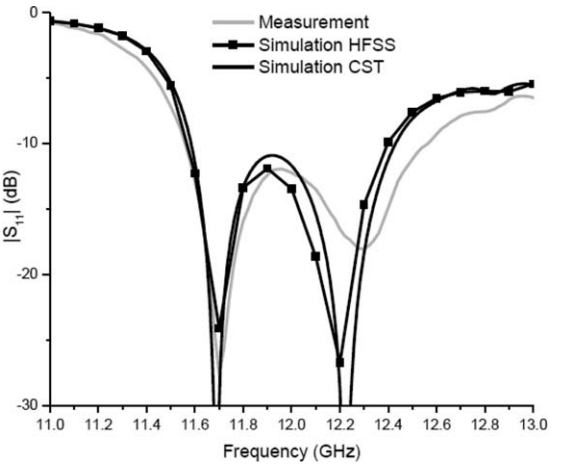

Figure 9 Simulated and measured $|S_{11}|$

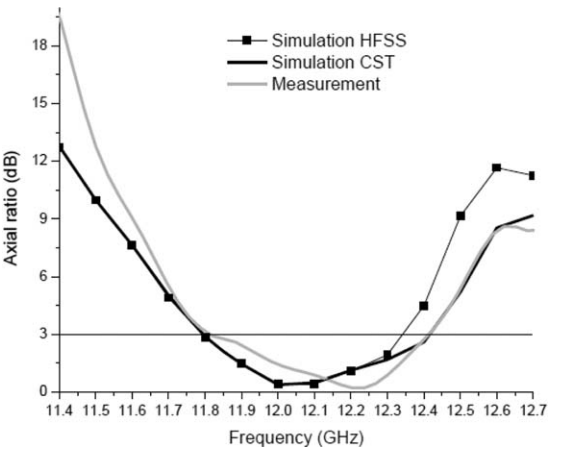

Figure 10 Simulated and measured axial ratios in the broadside direction, i.e., z-axis as a function of frequency

$$\Delta\phi_2 = 2\pi\ L_4/\lambda_g \tag{2}$$

where $\lambda_g = \lambda_0/(\varepsilon_r)^{1/2}$ is the guided wavelength.

Then, the total phase difference of E_θ and E_φ can be calculated as:

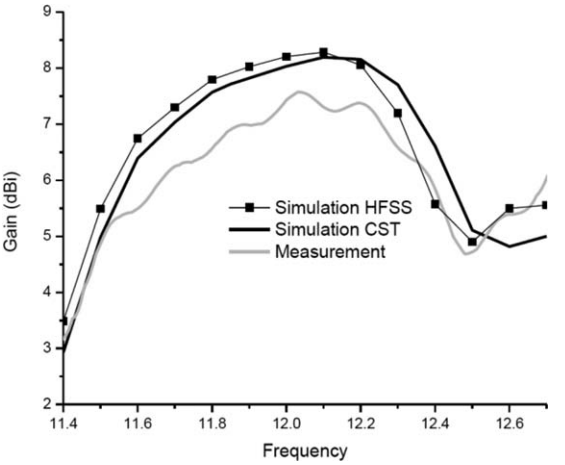

Figure 11 Simulated and measured gains in the broadside direction, i.e., z-axis as a function of frequency

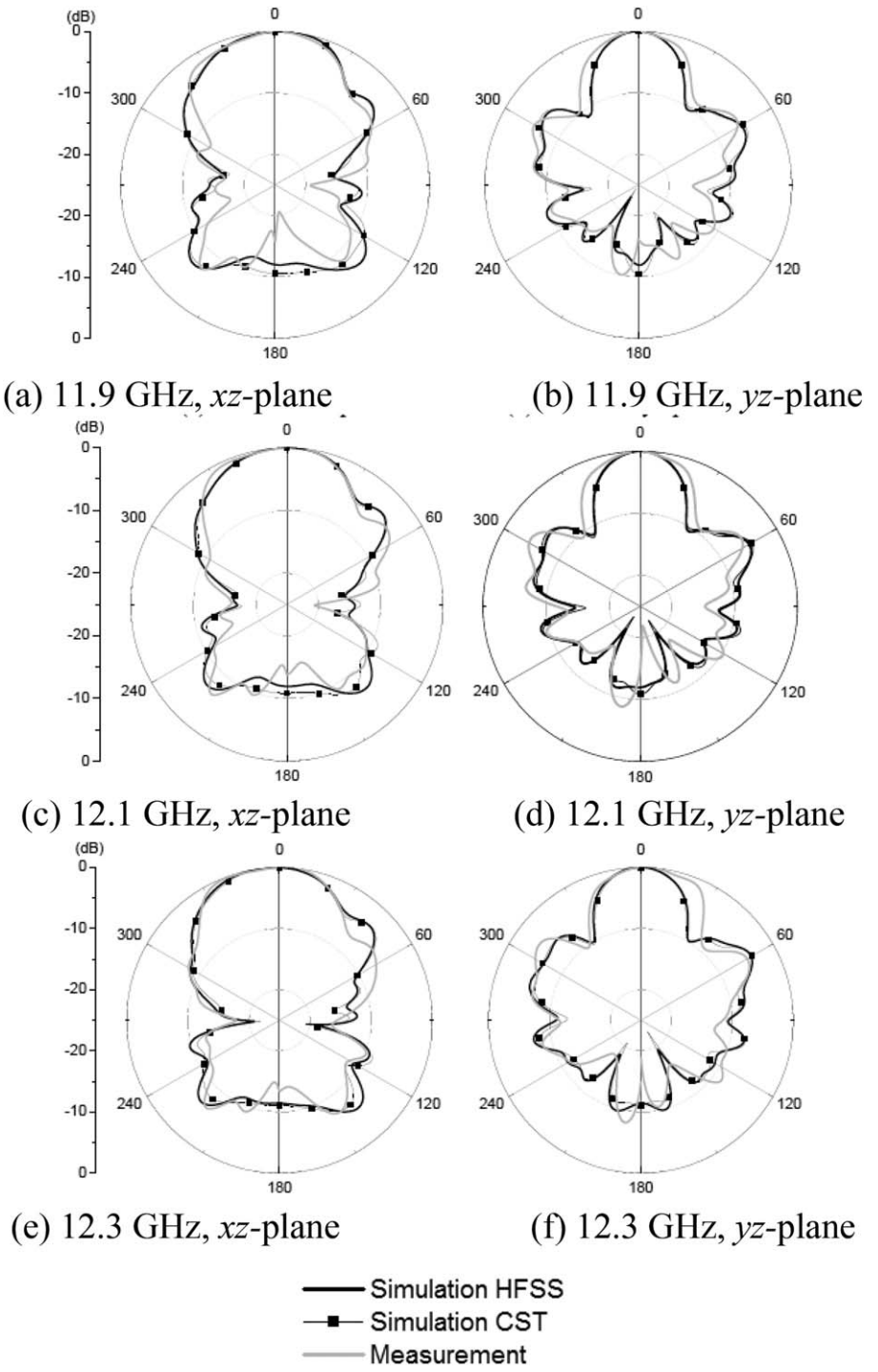

Figure 12 Simulated and measured normalized radiation patterns

$$\Delta\phi=\Delta\phi_1+\Delta\phi_2 \tag{3}$$

To achieve CP along the z-axis, we require that

$$\Delta\phi=\pi/2 \tag{4}$$

According to (1)–(4), the distance between the dipole and the aperture can be calculated as

$$L_4=0.25\left(\lambda_0\lambda_g\right)/\left(\lambda_0-\lambda_g\right) \tag{5}$$

As such, all of the dimensional parameters of the antenna in Figure 3 can be determined, and they are tabulated in Table 1.

To understand how the position and length of the dipole antenna affect the overall antenna performance, a parametric study is presented using Ansoft HFSS. When one parameter is investigated, the others are kept constant. The results provide useful guidelines for practical designs.

Figure 4 shows the phase difference $\left(\angle E_\theta-\angle E_\varphi\right)$ and the magnitude ratio ($|E_\theta|/|E_\varphi|$) in the broadside direction, i.e., the z-axis, as a function of L_d. As L_d increases, both the phase difference and magnitude ratio decrease. When L_d =6.5 mm, E_θ and E_φ have almost the same magnitude and 90° phase difference. Figure 5 exhibits axial ratios in the broadside direction, i.e., the z-axis, as a

function of frequency versus different values of L_d. Widest axial ratio bandwidth is achieved when $L_d = 6.5$ mm.

The effect of the distance between the dipole and the aperture (L_4) in the broadside direction, i.e., the z-axis, on the phase difference ($\angle E_\theta - \angle E_\varphi$) and the magnitude ratio ($|E_\theta|/|E_\varphi|$) are presented in Figure 6. With increasing L_4, the phase difference decreases whereas the magnitude ratio increases. When $L_4 = 13$ mm, E_θ and E_φ have almost the same magnitude and 90° phase difference. As shown in Figure 7, the widest axial ratio bandwidth is obtained when $L_4 = 6.5$ mm.

In this way, we can optimize the axial ratio by adjusting the two parameters L_4 and L_d as follows:

1. If we want to increase the phase difference but keep the magnitude ratio stable, we can decrease L_4 and L_d simultaneously.
2. If we want to increase the magnitude ratio but keep the phase difference stable, we should increase L_4 and decrease L_d.
3. If we want to decrease the phase difference but keep the magnitude ratio stable, we can increase L_4 and L_d simultaneously.
4. If we want to decrease the magnitude ratio but keep the phase difference stable, we should increase L_d and decrease the L_4.

Based on this investigation, $L_d = 6.5$ mm and $L_4 = 13$ mm are selected to achieve low axial ratio.

3. RESULTS AND DISCUSSION

To verify the design procedure, we first repeat the simulation in CST and then fabricate and measure the proposed antenna. Figure 8 depicts depicts photographs of the top and bottom views of the antenna prototype. Experimental results together with simulation in both CST and HFSS are shown in Figures 9–12. Good agreement between experiments and simulations is observed. Figure 9 shows the reflection coefficients, and a measured value of |S11| less than −10 dB is achieved in the band of 11.6–12.5 GHz. The axial ratio in the broadside direction is shown in Figure 10. The measured axial ratio is less than 3 dB between 11.8 GHz and 12.4 GHz.

It can be seen from Figure 11 that the maximum measured gain is 7.5 dBi and, in the effective band of 11.8–12.4 GHz, the measured gain is higher than 6.2 dBi. Note that with the employment of the horn antenna instead of printed magnetic dipoles, the gain of the proposed antenna is significantly higher than those in Refs. [13,14]. Radiation patterns at 11.9 GHz, 12.1 GHz and 12.3 GHz in both the xz- and yz-planes are shown in Figure 12 and end-fire beams are observed.

4. CONCLUSION

A circularly polarized (CP) SIW horn antenna combined with a dipole is proposed. The principle of the antenna is explained, and a parametric study provides dipole design guidelines for CP operation. Measurements of a prototype at 12 GHz validate the design approach. In the relative effective bandwidth of 5%, the proposed antenna is demonstrated to exhibit high gain, low axial ratio, good impedance match as well as directive CP beams in the plane of the substrate. Due to the Potter horn and dipole designs, the achieved gain is significantly higher than those of previously reported similar antennas. This SIW CP horn antenna is a good candidate for applications in broadcasting satellite services.

ACKNOWLEDGMENT

This work was supported by the Natural Sciences and Engineering Research Council of Canada.

REFERENCES

1. ITU, Radio Regulations, Article 5, Frequency allocations, Jan. 2009.
2. S. Gao, Q. Luo, and F. Zhu, Circularly polarized antennas, Wiley-IEEE Press, New York, 2013.
3. M. Bozzi, A. Georgiadis, and K. Wu, Review of substrate-integrated waveguide circuits and antennas, IET Microwave Antenna Propag 5 (2011), 909–920.
4. Z.L. Li and K. Wu, A new approach to integrated horn antenna, Proc Int Symp Antenna Technol Appl Electromagn (2004), 535–538.
5. H. Wang, D.G. Fang, B. Zhang, and W.Q. Che, Dielectric loaded substrate integrated waveguide (SIW) H-plane horn antennas, IEEE Trans Antenna Propag 58 (2010), 640–647.
6. M. Esquius-Morote, B. Fuchs, J. Zürcher, and J.R. Mosig, A printed transition for matching improvement of SIW horn antennas, IEEE Trans Antenna Propag 61 (2013), 1923–1930.
7. L. Wang, X.X. Yin, S.L. Li, H.X. Zhao, L.L. Liu, and M. Zhang, Phase corrected substrate integrated waveguide H-plane horn antenna with embedded metal-via arrays, IEEE Trans Antennas Propag 62 (2014), 1854–1861.
8. G.Q. Luo, Z.F. Hu, Y. Liang, L.Y. Yu, and L.L. Sun, Development of low profile cavity backed crossed slot antennas for planar integration, IEEE Trans Antenna Propag 57 (2009), 2972–2979.
9. D.Y. Kim, J.W. Lee, T.K. Lee, and C.S. Cho, Design of SIW cavity-backed circular- polarized antennas using two different feeding transitions, IEEE Trans Antenna Propag 59 (2011), 1398–1403.
10. C. Jin, Z. Shen, R. Li, and A. Alphones, Compact circularly polarized antenna based on quarter-mode substrate integrated waveguide sub-array, IEEE Trans Antennas Propag 62 (2014), 963–967.
11. S.A. Razavi and M.H. Neshati, Development of a low-profile circularly polarized cavity-backed antenna using HMSIW technique, IEEE Trans Antenna Propag 61 (2013), 1041–1047.
12. R.M. Cox and W.E. Rupp, Circularly polarized phased array antenna element, IEEE Trans Antenna Propag 18 (1970), 804–807.
13. W.J. Lu, J.W. Shi, K.F. Tong, and H.B. Zhu, Planar end fire circularly polarized antenna using combined magnetic dipoles, IEEE Antenna Wireless Propag Lett 14 (2015), 1263–1266.
14. W.H. Zhang, W.J. Lu, and K.W. Tam, A planar end-fire circularly polarized complementary antenna with beam in parallel with its plane, IEEE Trans Antenna Propag 64 (2016), 1146–1152.
15. R.N. Simons, Coplanar waveguide circuits, components, and systems, Wiley-IEEE Press, New York, 2001.

15 GHz GRID ARRAY ANTENNA FOR 5G MOBILE COMMUNICATIONS SYSTEM

Muhammad Sani Yahya and S.K.A. Rahim
Wireless Communication Centre (WCC), Universiti Teknologi Malaysia, Johor Bahru, Johor 81310, Malaysia; Corresponding author: symuhammad2@live.utm.my, sharulkamal@fke.utm.my

Received 23 May 2016

ABSTRACT: *A compact grid array antenna implemented using FR4 substrate for 5G Mobile Communications at 15 GHz is presented. The antenna with dimensions of 49 mm × 58 mm × 1.6 mm has 23 radiating elements to provide high gain. It is excited using coaxial feeding technique. Measurement of the fabricated prototype for the simulated antenna was carried out. Both measured and simulated results agree with each other. The measured result shows that the antenna has achieved an impedance bandwidth of 14% from 13.8 GHz to 15.9 GHz with a gain of 14.4 dBi at 15.9 GHz.* © 2016 Wiley Periodicals, Inc.

Microwave Opt Technol Lett 58:2977–2980, 2016; View this article online at wileyonlinelibrary.com. DOI 10.1002/mop.30190

Key words: *5G; mobile communications; coaxial probe; grid array antenna*

1. INTRODUCTION

The contemporary fourth generation (4G) wireless communication systems and antennas [1–3] used in several countries around